Inorganic Chemistry

Article

pubs.acs.org/IC

# Enhanced Photoluminescence and Thermal Properties of Size Mismatch in $Sr_{2.97-x-y}Eu_{0.03}Mg_xBa_ySiO_5$ for High-Power White Light-Emitting Diodes

Zhipeng Ci,* Meidan Que, Yurong Shi, Ge Zhu, and Yuhua Wang*

Department of Materials Science, School of Physical Science and Technology, Lanzhou University, Lanzhou 730000, China

Supporting Information

**ABSTRACT:** In this Study, $Mg^{2+}$ and $Ba^{2+}$ act to enhance the maximum emission of $Sr_{2.97}SiO_5$:0.03$Eu^{2+}$ significantly and redshift the emission band to the orange-red region in $Sr_{2.97-x-y}Mg_xBa_ySiO_5$:0.03$Eu^{2+}$. Size mismatch between the host and the doped cations tunes the photoluminescence spectra shift systematically. A slight blue shift when increasing the amount of $Mg^{2+}$ occurs in the $Sr_{2.97-x}Eu_{0.03}Mg_xSiO_5$ lattices, and a rapid red shift occurs when $Ba^{2+}$ is codoped in the $Sr_{2.57-y}Eu_{0.03}Mg_{0.4}Ba_ySiO_5$ lattices. The emission spectra were tuned from 585 to 601 nm by changing the concentration of $Ba^{2+}$. Accordingly, we propose the underlying mechanisms of the changes in the photoluminescence properties by adjusting the cation composition of phosphors. The influence of the size mismatch on the thermal quenching is also observed. This mechanism could be widely applied to oxide materials and could be useful in tuning the photoluminescence properties, which are sensitive to local coordination environment. The emission bands of $Sr_{2.97-x-y}Eu_{0.03}Mg_xBa_ySiO_5$ show the blue shift with increasing temperature, which could be described in terms of back tunneling of the excited electrons from the low-energy excited state to the high-energy excited state. Thus, the $Sr_{2.97-x-y}Eu_{0.03}Mg_xBa_ySiO_5$ phosphors could have potential applications in the daylight LEDs or warm white LEDs.

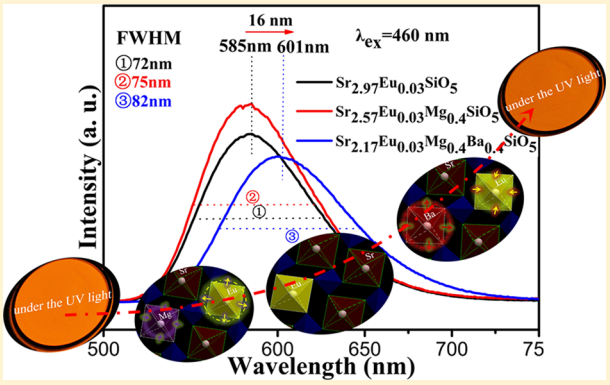


## 1. INTRODUCTION

White light-emitting diodes (LEDs) are considered to be next-generation solid-state lighting systems because of their excellent properties such as high luminous efficiency, energy saving, long lifetime, and lack of toxic mercury. They are the ideal replacement of conventional incandescent and fluorescent lamps in the near future. White LEDs can be fabricated by modulating the lights from red, green, and blue color-emitting LED chips or by combining color-converting phosphors with LEDs (pc-LEDs).[1,2] There are three types of pc-LEDs;[3−5] a blue-emitting LED (InGaN) coated with a yellow phosphor ($Ce^{3+}$-doped $(Y,Gd)_3(Al,Ga)_5O_{12}$ (YAG:$Ce^{3+}$)) is the most common one due to a low fabrication cost and high luminescence efficiency.[6,7] Nevertheless, the obtained white light shows a cool white with a color temperature of about 5000 K, which is due not only to the lack of emission in the red component, further resulting in an inferior white light compared to incandescent bulbs, but also to the lack of thermal stability at elevated temperatures during white LED operation when pumped by a blue LED chip. These are significant obstacles to overcome before achieving the transition to solid-state lighting. White LEDs using a near-ultraviolet (n-UV) LED (350−420 nm) with three primary color emissions mixed with three individual red, green, and blue-emitting phosphors have been investigated to improve the color rendering index value.[8,9] Accordingly, the eventual performance of white LED-based devices strongly depends on the luminescence properties of the phosphor used.[10,11] Therefore the researches on phosphors excitable by the n-UV light are rapidly increasing and have become one of the hot research topics in the phosphor community.[12,13]

The $Sr_3SiO_5$:$Eu^{2+}$ phosphor emits a yellow light and has been attracting a lot attention due to the application in white LEDs. The combination of the UV LEDs, $Sr_3SiO_5$:$Eu^{2+}$, and other color-emitting phosphors yields superior luminous efficiency and high color stability.[14] Up to now, $Sr_3SiO_5$:$Eu^{2+}$ studies have focused on the effect of $Eu^{2+}$ concentration,[15] various fluxing agents,[16] and so on.[17−24] However, the color rendering of as-prepared $Sr_3SiO_5$:$Eu^{2+}$ is not perfectly satisfactory for white LED applications because its emission lacks the high efficiency and longer wavelength emission that are needed. Consequently, another purpose is to enhance the red emission component to meet the needs of warm-white LEDs. Shen et al. reported a phosphor of $Ba^{2+}$-codoped $Sr_3SiO_5$:$Ce^{3+}$, $Li^+$.[25] The research implies that $Ba^{2+}$ plays a significant role in enhancing the red-emitting component in the emission band. Yet, the mechanism of the emission shift has not been reasonably explained. In this Work, we synthesized a series of $Sr_{2.97-x-y}Eu_{0.03}Mg_xBa_ySiO_5$ ($x$, $y$ = 0.1, 0.2, 0.3, 0.4, 0.5, 0.6) compounds sintered at 1400−

**Received:** November 17, 2013
**Published:** January 28, 2014

   dx.doi.org/10.1021/ic402859s | Inorg. Chem. 2014, 53, 2195−2199

1500 °C, investigated the photoluminescence properties and the thermal stability of those compounds, and then explained the mechanism of emission shift due to the introduction of $Mg^{2+}$ and $Ba^{2+}$ into $Sr_{2.97}SiO_5$:0.03$Eu^{2+}$. Besides, the work of adding a trace of P, Ge, and Al and replacing Si with K and Y as charge compensation was conducted, and the related effect on thermal stability was presented.

## 2. EXPERIMENTAL METHODS

All raw materials were purchased from Topstar except $SiO_2$, and were used without further treatment. The typical synthetic procedure is shown as follows. The appropriate stoichiometric mixture of $SrCO_3$ (99.99%), $SiO_2$ (99.8%), MgO (99.99%), $BaCO_3$ (99.99%), and $Eu_2O_3$ (99.99%) was weighted and mixed thoroughly using ethanol as a solvent. Then the powder was annealed at 1400−1500 °C for 4 h in a corundum crucible with the atmosphere of $N_2/H_2$ = 95:5%. The as-prepared samples were cooled to the room temperature naturally and were orange in body color with sporadic yellow-green spots, possibly from $Sr_2SiO_4$:$Eu^{2+}$, in the surface. After discarding the top layer of the nongrinded products, the interior of the samples shows uniform orange without yellow-green spots, and eventually, the uniform orange samples required were obtained.

The crystal structures of the synthesized samples were identified by using a Rigaku D/Max-2400 X-ray diffractometer (XRD) with Ni-filtered Cu K$\alpha$ radiation. The photoluminescence (PL), photoluminescence excitation (PLE), and temperature-dependent photoluminescence spectra of the samples were measured using an FLS-920T fluorescence spectrophotometer equipped with a 450 W Xe light source and double excitation monochromators. All of the measurements were performed at room temperature. Thermal quenching was tested using a heating apparatus (TAP-02) in combination with PL equipment.

## 3. RESULTS AND DISCUSSION

The XRD patterns of the $Sr_{2.97}Eu_{0.03}SiO_5$, $Sr_{2.57}Eu_{0.03}Mg_{0.4}SiO_5$, and $Sr_{2.17}Eu_{0.03}Mg_{0.4}Ba_{0.4}SiO_5$ phosphors synthesized by the solid-state reaction methods are shown in Figure 1. The as-prepared phosphors form a pure $Sr_3SiO_5$ phase, which are well indexed to JCPDF card no. 26−0984. Figure 1b shows the detailed XRD patterns from 29.5° to 32.5°. Since the radius of $Mg^{2+}$ is smaller than that of $Sr^{2+}$, with the doping of $Mg^{2+}$, the diffraction peaks of the $Sr_{2.57}Eu_{0.03}Mg_{0.4}SiO_5$ phosphor show an obvious shift to larger 2$\theta$ angles compared to that of the pure $Sr_{2.97}Eu_{0.03}SiO_5$. In addition, the strong and sharp diffraction peaks indicate that the $Sr_{2.57}Eu_{0.03}Mg_{0.4}SiO_5$ phosphor is highly crystallized, which benefits the luminescence perfomance.[26] However, the radius of $Ba^{2+}$ is bigger than that of $Mg^{2+}$ and $Sr^{2+}$, and the diffraction peaks shift to smaller 2$\theta$ angles when $Ba^{2+}$ is doped into $Sr_{2.57-x}Eu_{0.03}Mg_{0.4}Ba_xSiO_5$. Finally, the peaks of the $Sr_{2.17}Eu_{0.03}Mg_{0.4}Ba_{0.4}SiO_5$ phosphor are located between that of the $Sr_{2.97}Eu_{0.03}SiO_5$ phosphor and that of the $Sr_{2.57}Eu_{0.03}Mg_{0.4}SiO_5$ phosphor. The surplus Mg series and Ba series of the powder XRDs are shown in Supporting Information, Figures S1 and S2.

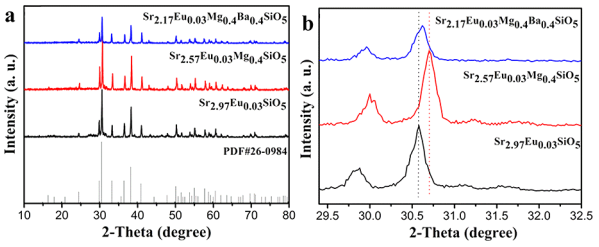


**Figure 1.** (a) The XRD patterns of the as-prepared samples $Sr_{2.97}Eu_{0.03}SiO_5$, $Sr_{2.57}Eu_{0.03}Mg_{0.4}SiO_5$, and $Sr_{2.17}Eu_{0.03}Mg_{0.4}Ba_{0.4}SiO_5$, sintered at 1450 °C. (b) The detailed XRD patterns ranging from 29.5° to 32.5° for the samples $Sr_{2.97}Eu_{0.03}SiO_5$, $Sr_{2.57}Eu_{0.03}Mg_{0.4}SiO_5$, and $Sr_{2.17}Eu_{0.03}Mg_{0.4}Ba_{0.4}SiO_5$, sintered at 1450 °C.

Figure 2a shows the emission spectra of $Sr_{2.97}Eu_{0.03}SiO_5$, $Sr_{2.57}Eu_{0.03}Mg_{0.4}SiO_5$, and $Sr_{2.17}Eu_{0.03}Mg_{0.4}Ba_{0.4}SiO_5$. All samples present a broad-band emission originated from the 5d→4f transition of $Eu^{2+}$ due to the strong coupling of the 5d electron with the host lattice. The full width at half-maximum (FWHM) of the Mg series and Ba series has progressively broadened compared to that of $Sr_{2.97}Eu_{0.03}SiO_5$. $Sr_{2.57}Eu_{0.03}Mg_{0.4}SiO_5$ exhibits stronger emission intensity from 500 to 750 nm than that of $Sr_{2.97}Eu_{0.03}SiO_5$, which is due to the better crystallinity (seen in Figure 1). The relative PLE spectra of $Sr_{2.97-x}Eu_{0.03}Mg_xSiO_5$ and $Sr_{2.57-y}Eu_{0.03}Mg_{0.4}Ba_ySiO_5$ cover from UV to blue light, as shown in Figure 2b,c, respectively. The relative PL spectra of $Sr_{2.97-x}Eu_{0.03}Mg_xSiO_5$ slightly shift to a shorter wavelength when the amount of $Mg^{2+}$ increases, which is consistent with the observation of the PLE spectra, as shown in Figure 2d. Conversely, Figure 2e presents that the PL spectra have a rapid redshift from 585 to 601 nm, and concentration quenching occurs when the $Ba^{2+}$ concentration is beyond 0.4. The reasons of the spectra shift could be explained by the following mechanism.

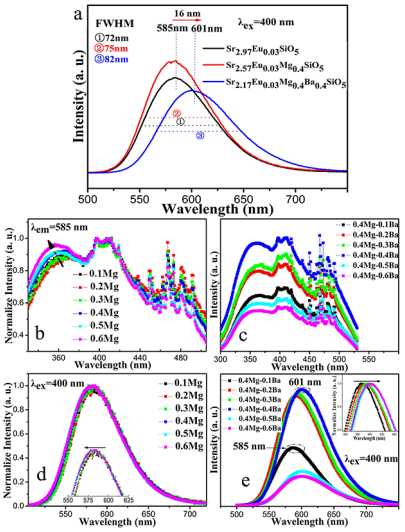


**Figure 2.** (a) The room-temperature PL spectra of $Sr_{2.97}Eu_{0.03}SiO_5$, $Sr_{2.57}Eu_{0.03}Mg_{0.4}SiO_5$, and $Sr_{2.17}Eu_{0.03}Mg_{0.4}Ba_{0.4}SiO_5$, excited at 400 nm. (b,c) The relative PLE spectra of $Sr_{2.97-x}Eu_{0.03}Mg_xSiO_5$ ($x$ = 0.1, 0.2, 0.3, 0.4, 0.5, 0.6) and $Sr_{2.57-y}Eu_{0.03}Mg_{0.4}Ba_ySiO_5$ ($y$ = 0.1, 0.2, 0.3, 0.4, 0.5, 0.6), monitored at 585 nm and the separate maximum emission wavelength. (d,e) The relative room-temperature PL spectra of $Sr_{2.97-x}Eu_{0.03}Mg_xSiO_5$ and $Sr_{2.57-y}Eu_{0.03}Mg_{0.4}Ba_ySiO_5$, excited at 400 nm.

In the $Sr_{2.97-x-y}Eu_{0.03}Mg_xBa_ySiO_5$ structure, the $[EuO_6]^{10-}$ octahedral neighbors with the $[MgO_6]^{10-}$, $[SrO_6]^{10-}$, or $[BaO_6]^{10-}$ octahedrals by linking to the $[SiO_4]^{4-}$ tetrahedral. From the point of view of reference 27, the photoluminescence property significantly interrelates with local coordination environment.


dx.doi.org/10.1021/ic402859s | Inorg. Chem. 2014, 53, 2195−2199

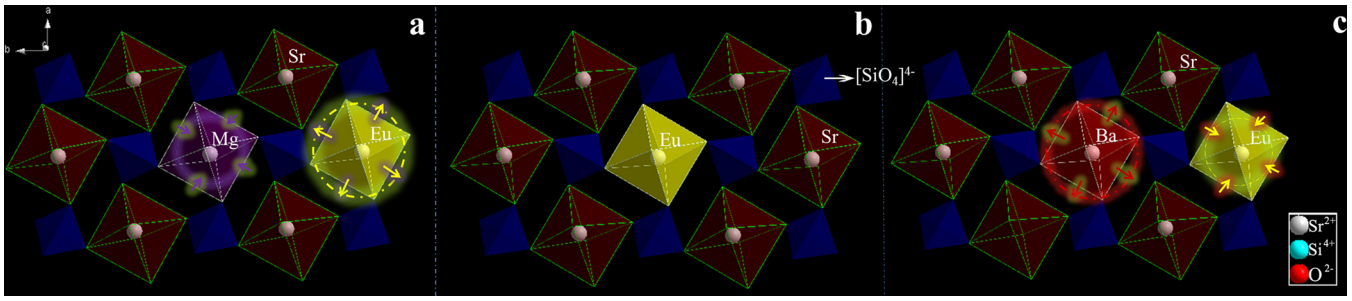


**Figure 3.** The crystal structure of the $Sr_{2.97-x-y}Eu_{0.03}Mg_xBa_ySiO_5$ phosphors; the detailed $Eu^{2+}$ crystal site environments: (a) the $[MgO_6]^{10-}$ octahedral neighbors with the $[EuO_6]^{10-}$ octahedral, (b) the $[SrO_6]^{10-}$ octahedral neighbors with the $[EuO_6]^{10-}$ octahedral, and (c) the $[BaO_6]^{10-}$ octahedral neighbors with the $[EuO_6]^{10-}$ octahedral by linking to the $[SiO_4]^{4-}$ tetrahedral.

As shown in Figure 3(a), the $[MgO_6]^{10-}$ octahedral neighbors with the $[EuO_6]^{10-}$ octahedral by linking to the distorted $[SiO_4]^{4-}$ tetrahedral. This is because the radius of $Mg^{2+}$ is smaller than that of $Sr^{2+}$, thus the $[MgO_6]^{10-}$ octahedral lattice shrinks compared with the original $[SrO_6]^{10-}$ octahedral, the condition preferably leading to the neighboring $[EuO_6]^{10-}$ octahedral lattice expansion. Consequently, the length of the Eu−O bond becomes longer, which gives rise to the weaker nephelauxetic effect and the lower crystal field splitting of 5d orbitals,[28] and then causes a blueshift of the Mg series emission bands. Furthermore, the symmetry is decreased with the introduction of the doping ions and affects the preferential orientation of a $Eu^{2+}$ d orbital, so that the $Eu^{2+}$emission shifts to a longer wavelength.[29] Eventually, as a comprehensive result of the three factors, it is found that the emission bands shift slightly to a shorter wavelength region, as shown in Figure 2d.

As shown in Figure 3b, the $[SrO_6]^{10-}$ octahedral neighbors with the $[EuO_6]^{10-}$ octahedral by linking to the distorted $[SiO_4]^{4-}$ tetrahedral. In this condition, even though $Mg^{2+}$ and $Ba^{2+}$ are introduced into $Sr_{2.97}SiO_5$:0.03$Eu^{2+}$, the crystal environment of $Eu^{2+}$ in $Sr_{2.97-x-y}Eu_{0.03}Mg_xBa_ySiO_5$ should be also similar to that in $Sr_{2.97}SiO_5$:0.03$Eu^{2+}$ on the local scale.[30] Thereby, the two PL spectra of $Eu^{2+}$ in both $Sr_{2.97}SiO_5$ and $Sr_{2.97-x-y}Mg_xBa_ySiO_5$ are similar.

As shown in Figure 3c, the $[BaO_6]^{10-}$ octahedral neighbors with the $[EuO_6]^{10-}$ octahedral by linking to the distorted $[SiO_4]^{4-}$ tetrahedral. This case is different; the radius of $Ba^{2+}$ is larger than that of $Sr^{2+}$, and the $[BaO_6]^{10-}$ octahedral induces lattice expansion, which leads to the neighboring $[EuO_6]^{10-}$ octahedral lattice shrink. The length of the Eu−O bond becomes shorter, enhances the nephelauxetic effect, and enlarges the crystal field splitting of 5d orbitals of $Eu^{2+}$. Identically, the symmetry is also decreased with the introduction of the doping ions and affects the preferential orientation of a $Eu^{2+}$ d orbital, so that the $Eu^{2+}$emission shifts to a longer wavelength. Eventually, the three factors all result in the redshift of the emission peaks. In this Work, we can observe an obvious redshift in Figure 2e. Besides the above three causes, the Stokes shift is also an impartment factor that influences the spectra shift.

A comprehensive understanding of the thermal quenching of phosphors used in LEDs is indispensable because high-power LEDs suffer from thermal problems. Numerous investigations have discussed the thermal quenching behaviors.[31−35] Two competing factors prevail; one is the activation energy of nonradiative relaxation, and the other is the rate of temperature-induced direct tunneling, which prevents emissive transition between the different activator ions excited state and the ground state in host.[36]

The temperature-dependent PL spectra of $Sr_{2.97}Eu_{0.03}SiO_5$, $Sr_{2.57}Eu_{0.03}Mg_{0.4}SiO_5$, and $Sr_{2.17}Eu_{0.03}Mg_{0.4}Ba_{0.4}SiO_5$ excited at 400 nm are shown in Figure 4a,b,c, respectively. The thermal

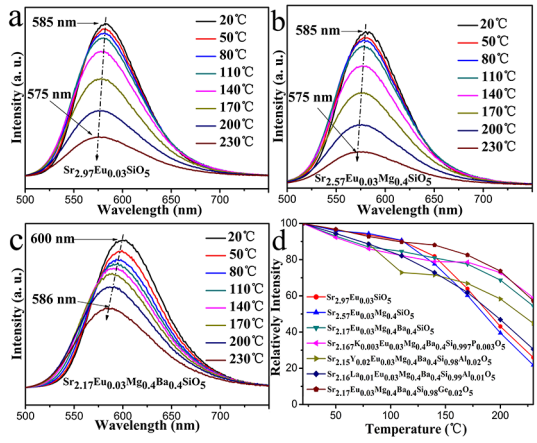


**Figure 4.** The PL spectra of (a) $Sr_{2.97}Eu_{0.03}SiO_5$, (b) $Sr_{2.57}Eu_{0.03}Mg_{0.4}SiO_5$, and (c) $Sr_{2.17}Eu_{0.03}Mg_{0.4}Ba_{0.4}SiO_5$ phosphors under various temperatures. (d) The dependence of normalized PL intensities on temperature for phosphors, excited at 400 nm.

quenching behavior of photoluminescence is measured from 20 to 230 °C. The emission intensities of all samples gradually decline. The emission intensity of $Sr_{2.97}Eu_{0.03}SiO_5$ decreases faster with increasing temperature than that of $Sr_{2.17}Eu_{0.03}Mg_{0.4}Ba_{0.4}SiO_5$, while much more slowly than that of $Sr_{2.57}Eu_{0.03}Mg_{0.4}SiO_5$. It indicates that the doping of $Ba^{2+}$ makes a contribution to the thermal stability, but the doping of $Mg^{2+}$ brings the opposite result. It can be explained by the configurational coordinate diagram in Figure 5. The curve g is the ground state of $Eu^{2+}$. The curves $e_1$, $e_2$, and $e_3$ are the excited states of the $Eu^{2+}$ of the $[EuO_6]^{10-}$ octahedral neighboring with the $[SrO_6]^{10-}$, $[MgO_6]^{10-}$, and $[BaO_6]^{10-}$ octahedrals, respectively. $\Delta R$ is the departure from the ground state to the excited states along the $R$ axis. A, B, and C are the crossing points of g and $e_1$, $e_2$, and $e_3$, respectively. F, G, and E are the lowest positions of the $e_1$, $e_2$, and $e_3$ curves, respectively. $\Delta E_1$, $\Delta E_2$, and $\Delta E_3$ are the energy differences of F to A, G to B, and E to C, respectively. In our Experiment, the concentration of $Eu^{2+}$ is quite low (1%), and thus the distance between $Eu^{2+}$ and $Eu^{2+}$ is larger. To simplify the question, we assume the $Eu^{2+}$ is noninteracting. Under blue or UV light, the electrons are excited to the excited states from g to $e_1$, $e_2$, and $e_3$. At the room


dx.doi.org/10.1021/ic402859s | Inorg. Chem. 2014, 53, 2195−2199

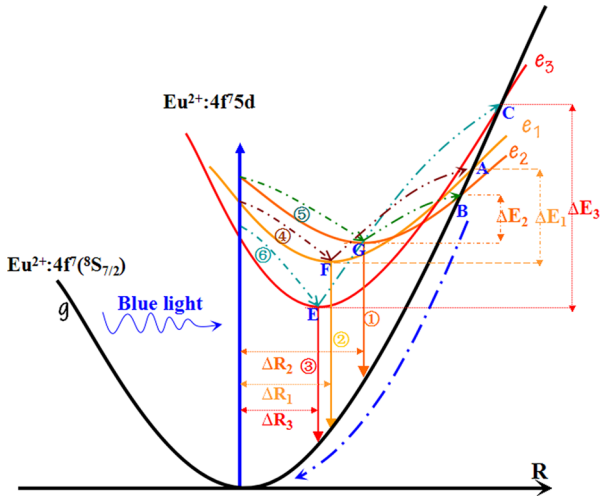


**Figure 5.** The configurational coordinate diagram of the ground state of $Eu^{2+}$ and the excited states of $Eu^{2+}$ located in the three different crystal environments.

temperature, most of the electrons return to the ground state along ways ①, ②, and ③. But with the increasing of temperature, more electrons return to the ground along ways ④, ⑤, and ⑥ from the crossing points A, B, and C due to the electron−phonon coupling. In our Experiment, the doping of the $Mg^{2+}$ and $Ba^{2+}$ greatly changes the crystal field and the nephelauxetic effect, then affects the position of the crossing points A, B, and C of the ground state and excited states; furthermore the doping determines the value of $\Delta E$. According to the results of the thermal properties in our Experiment, the mechanism of the thermal quenching is illustrated in Figure 5; the crossing point B is located below the crossing point A, and the crossing point C is above the crossing point A, that is, $\Delta E_3 > \Delta E_1 > \Delta E_2$. Therefore, the doping of $Ba^{2+}$ is beneficial to the thermal properties, and the doping of $Mg^{2+}$ is not.

The FWHMs of the three samples are widened with increasing temperature, and this widening can be interpreted by using the Boltzmann distribution according to the following equations:[37]

$$\mathrm{FWHM}(T) = W_0\sqrt{\coth\left(\frac{hw}{2kT}\right)} \quad (1)$$

$$W_0 = \sqrt{8\ln 2}\,(hw)\sqrt{S} \quad (2)$$

where $W_0$ is the FWHM at 0 °C, $hw$ is the energy of the lattice vibration that interacts with the electronic transitions, $S$ is the Huang−Rhys−Pekar parameter, and $k$ is the Boltzmann constant ($k = 8.629 \times 10^{-5}$ eV). It is assumed that $hw$ is the same for the $4f^7$ ground state and the $4f^65d$ excited state of $Eu^{2+}$. As the temperature increases, the thermally activated luminescent center strongly interacts with the thermally active phonon, the population density of phonon is increased, the electron−phonon interaction is dominant, and consequently the FWHMs of emission spectrum are broadened.[38−40] Meanwhile, the peak positions of emission spectra blueshift with the increasing temperature. At 20 and 230 °C, for the $Sr_{2.97}Eu_{0.03}SiO_5$ compound, the peak positions of emission spectra are about 585 and 575 nm, respectively; for the $Sr_{2.57}Eu_{0.03}Mg_{0.4}SiO_5$ compound, the peak positions are also about 585 and 575 nm, respectively; and for the $Sr_{2.17}Eu_{0.03}Mg_{0.4}Ba_{0.4}SiO_5$ compound, the peak positions are about 600 and 586 nm, respectively. To account for this observation, consider that thermally active phonon-assisted tunneling from the excited states of low-energy emission band to the excited states of high-energy emission band in the configuration coordinate diagram occurs.[40,41] The phosphor $Sr_{2.97-x-y}Eu_{0.03}Mg_xBa_ySiO_5$ has two different cation sites in the lattice, Sr(I) and Sr(II), and results in two emission bands: Eu(I) and Eu(II). Hence, the PL spectra of $Sr_{2.97-x-y}Eu_{0.03}Mg_xBa_ySiO_5$ are composed of two emission bands: Eu(I) of shorter wavelength emission and Eu(II) of longer wavelength emission. As the Sr(I) and Sr(II) sites are both 6-coordinated with similar local coordination environments, two emission bands of Eu(I) and Eu(II) are similar, resulting in a single overlap emission band in the emission spectra. Two emission bands (Eu(I) and Eu(II)) arise from different minima on the potential energy surface of relaxed excited state, as given in reference 41. At the low temperature, the barrier (Eu(I) to Eu(II)) is overcome, and the low-energy emission (Eu(II)) is dominant. At the higher temperature, the thermal back-transfer over the barrier (Eu(II) to Eu(I)) is possible, and consequently the higher energy emission (Eu(I)) is strengthened. Thus, the blueshift behavior is observed with the increasing temperature in our Work. Besides, the work of adding a trace of P, Ge, and Al to replace the Si element, with K, Y as charge compensation was conducted, and the related effect on thermal stability was presented clearly in Table 1. The PL spectra of surplus samples under various temperatures are shown in Supporting Information (Figures S3−S6). Compared to $Sr_{2.97}Eu_{0.03}SiO_5$, the thermal stability of $Sr_{2.57}Eu_{0.03}Mg_{0.4}SiO_5$ declines, but that of $Sr_{2.17}Eu_{0.03}Mg_{0.4}Ba_{0.4}SiO_5$ rapidly rises. On the basis of the $Sr_{2.17}Eu_{0.03}Mg_{0.4}Ba_{0.4}SiO_5$ compound, with trace Ge substituting for Si and P−K substituting for Si−Sr, the thermal stabilities of samples are lightly enhanced. But, with trace Al−Y or Al−La substituting for Si−Sr, the thermal stabilities of samples worsen.

**Table 1. Percentage of Temperature-Dependent Emission Intensities**

| | Eu | Eu, Mg | Eu, Mg, Ba | Eu, Mg, Ba, K−P | Eu, Mg, Ba, Y−Al | Eu, Mg, Ba, La−Al | Eu, Mg, Ba, Ge |
|---|---|---|---|---|---|---|---|
| **20** | 100% | 100% | 100% | 100% | 100% | 100% | 100% |
| **50** | 96.31% | 96.02% | 93.00% | 92.26% | 91.07% | 94.42% | 96.79% |
| **80** | 93.64% | 94.42% | 87.00% | 86.01% | 84.00% | 88.63% | 92.98% |
| **110** | 90.47% | 90.69% | 84.54% | 82.24% | 76.89 | 82.14% | 89.78% |
| **140** | 81.86% | 77.61% | 80.99% | 78.94% | 71.56% | 72.85% | 88.08% |
| **170** | 63.91% | 60.25% | 77.56% | 78.65% | 66.87% | 61.93% | 82.59% |
| **200** | 43.10% | 39.50% | 68.70% | 72.84% | 58.32% | 46.91% | 73.68% |
| **230** | 25.95% | 21.78% | 54.39% | 58.97% | 44.83% | 30.57% | 57.33% |


dx.doi.org/10.1021/ic402859s | Inorg. Chem. 2014, 53, 2195−2199

## 4. CONCLUSION

In summary, a simple solid-state route was adopted to prepare a series of oxide phosphors, $Sr_{2.97-x-y}Eu_{0.03}Mg_xBa_ySiO_5$ ($x$, $y$ = 0.1, 0.2, 0.3, 0.4, 0.5, 0.6), which could be used to tune the photoluminescence properties and thermal stability in the related size-mismatched cation-substituted phosphors. The PLE spectra span the UV to blue region, and the PL spectra show an orange-red emission. By the various crystal environments in the $Sr_{2.97-x-y}Eu_{0.03}Mg_xBa_ySiO_5$ structure, we try to explain the mechanisms of emission shift via adjusting the cation composition of phosphors. The emission peaks of $Sr_{2.97-x-y}Eu_{0.03}Mg_xBa_ySiO_5$ should have been influenced by the following factors: the nephelauxetic effect, the crystal field environment, the preferential orientation of the $Eu^{2+}$ d orbitals, and the Stokes shift. Studies have shown that the introduction of a certain amount of Mg and Ba or trace amounts of P, K, Ge, Al, Y, La could improve thermal stability. On the basis of these results, the orange-red emitting phosphors $Sr_{2.97-x-y}Eu_{0.03}Mg_xBa_ySiO_5$ could have potential application in blue or n-UV LEDs.

## ■ ASSOCIATED CONTENT

### Ⓢ Supporting Information

The surplus Mg series and Ba series of powder X-ray diffractions and the PL spectra of surplus samples under various temperatures are shown in Supporting Information. This material is available free of charge via the Internet at http://pubs.acs.org.

## ■ AUTHOR INFORMATION


### Corresponding Authors

*E-mail: cizhp@lzu.edu.cn (Z.C.).
*E-mail: wyh@lzu.edu.cn (Y.W.).


### Notes

The authors declare no competing financial interest.

## ■ ACKNOWLEDGMENTS

This work was supported by the National Science Foundation for Distinguished Young Scholars (No. 50925206), and the Research Fund for the Doctoral Program of Higher Education (No. 20120211130003).

## ■ REFERENCES


(1) Schubert, E. F.; Kim, J. K. *Science* **2005**, *308*, 1274−1278.
(2) Krames, M. R.; Shchekin, O. B.; Mueller-Mach, R.; Mueller, G. O.; Zhou, L.; Harbers, G.; Craford, M. G. *J. Disp. Technol.* **2007**, *3*, 160−175.
(3) Xie, R. J.; Hirosaki, N.; Mitomo, M.; Takahashi, K.; Sakuma, K. *Appl. Phys. Lett.* **2006**, *88*, 101−104.
(4) Yang, C. C.; Lin, C. M.; Chen, Y. J.; Wu, Y. T.; Chuang, S. R.; Liu, R. S.; Hu, S. F. *Appl. Phys. Lett.* **2007**, *90*, 123503−1−123503−3.
(5) Sheu, J. K.; Chang, S. J.; Kuo, C. H.; Su, Y. K.; Wu, L. W.; Lin, Y. C.; Lai, W. C.; Tsai, J. M.; Chi, G. C.; Wu, R. K. *IEEE Photonics Technol. Lett.* **2003**, *15*, 18−20.
(6) Bando, K.; Sakano, K.; Noguchi, Y.; Shimizu, Y. *J. Light Visual Environ.* **1998**, *22*, 1−2.
(7) Schlotter, P.; Baur, J.; Hielscher, C.; Kunzer, M.; Obloh, H.; Schmidt, R.; Schneider, J. *Mater. Sci. Eng., B* **1999**, *59*, 390−394.
(8) Lin, C. C.; Tang, Y. S.; Hu, S. F.; Liu, R. S. *J. Lumin.* **2009**, *129*, 1682−1684.
(9) Zhang, S. Y.; Nakai, Y.; Tsuboi, T.; Huang, Y. L.; Seo, H. J. *Inorg. Chem.* **2011**, *50*, 2897−2900.
(10) Wang, D. Y.; Huang, C. H.; Wu, Y. C.; Chen, T. M. *J. Mater. Chem.* **2011**, *21*, 10818−10822.
(11) Han, J. Y.; Im, W. B.; Kim, D.; Cheong, S. H.; Lee, G. Y.; Jeon, D. Y. *J. Mater. Chem.* **2012**, *22*, 5374−5381.
(12) Li, G. G.; Geng, D. L.; Shang, M. M.; Peng, C.; Cheng, Z. Y.; Lin, J. *J. Mater. Chem.* **2011**, *21*, 13334−13344.
(13) Liu, Y. F.; Zhang, X.; Hao, Z. D.; Wang, X. J.; Zhang, J. H. *Chem. Commun.* **2011**, *47*, 10677−10679.
(14) Park, J. K.; Kim, C. H.; Park, S. H.; Park, H. D. *J. Appl. Phys.* **2004**, *84*, 1647−1649.
(15) Li, P.; Yang, Z.; Wang, Z.; Guo, Q.; Li, X. *Chin. Sci. Bull.* **2008**, *53*, 974−977.
(16) Cheng, G.; Liu, Q.; Cheng, L.; Lu, L.; Sun, H.; Wu, Y.; Bai, Z.; Zhang, X.; Qiu, G. *J. Rare Earths* **2010**, *28*, 303−307.
(17) Sun, X. Y.; Zhang, J. H.; Zhang, X. *J. Appl. Phys.* **2009**, *105*, 013501−3.
(18) Jang, H. S.; Yang, H. S.; Kim, S. W.; Han, J. Y.; Lee, S. G. *Adv. Mater.* **2008**, *20*, 2696−2702.
(19) Jang, H. S.; Jeon, D. Y. *Opt. Lett.* **2007**, *32*, 3444−3446.
(20) Murray, C. B.; Norris, D. J.; Bawendi, M. G. *J. Am. Chem. Soc.* **1993**, *115*, 8706−8715.
(21) Jang, H. S.; Jeon, D. Y. *Appl. Phys. Lett.* **2007**, *90*, 041906.
(22) Luo, H. D.; Liu, J.; Zheng, X.; Han, L. X.; Han, K. X.; Yu, X. B. *J. Mater. Chem.* **2012**, *22*, 15887−15893.
(23) Eun, H. K.; Sung, W. C.; Su, E. C.; Ji, S. J.; Sung, H. K.; Seong, H. H. *J. Electrochem. Soc.* **2011**, *158*, 330−333.
(24) Nakamura, Y.; Watari, T.; Torikai, T.; Yada, M. *Mater. Sci. Eng.* **2011**, *18*, 102007.
(25) Shen, C. Y.; Li, K.; Yang, Y. *Proc. SPIE-OSA-IEEE* **2009**, *7635*, 76350K-1−76350K-6.
(26) Park, J. K.; Choi, K. J.; Yeon, J. H.; Lee, S. J.; Kim, C. H. *Appl. Phys. Lett.* **2006**, *88*, 043511−1−043511−3.
(27) Li, Y. Q.; Delsing, A. C. A.; deWith, G.; Hintzen, H. T. *Chem. Mater.* **2005**, *17*, 3242−3248.
(28) Peter, A. T.; Yau, Y. Y.; Li, X. N. *J. Phys. Chem. A.* **2013**, *117*, 2771−2781.
(29) Poort, S. H. M.; Van Krevel, J. W. H.; Stomphorst, R.; Vink, A. P.; Blasse, G. *J. Alloys Compd.* **1996**, *241*, 75−81.
(30) Xie, J. R.; Naoto, H.; Mamoru, M.; Takayuki, S.; Xin, X.; Hidehiko, T. *J. Am. Ceram. Soc.* **2005**, *88*, 2883−2888.
(31) Lin, C. C.; Xiao, Z. R.; Guo, G. Y.; Chan, T. S.; Liu, R. S. *J. Am. Chem. Soc.* **2008**, *43*, 5658−5659.
(32) Piao, X. Q.; Machida, K.; Horikawa, T.; Hanzawa, H.; Shimomura, Y.; Kijima, N. *Chem. Mater.* **2007**, *19*, 4592−4599.
(33) Li, Y. Q.; Hirosaki, N.; Xie, R. J.; Takeda, T.; Mitomo, M. *Chem. Mater.* **2008**, *20*, 6704−6714.
(34) Liu, W. R.; Yeh, C. W.; Huang, C. H.; Lin, C. C.; Chiu, Y. C.; Yeh, Y. T.; Liu, R. S. *J. Mater. Chem.* **2011**, *21*, 3740−3744.
(35) Piao, X. Q.; Horikawa, T.; Hanzawa, H.; Machida, K. *Appl. Phys. Lett.* **2006**, *88*, 161908−1−161908−3.
(36) Baginskiy, I.; Liu, R. S.; Wang, C. L.; Lin, R. T.; Yao, Y. J. *J. Electrochem. Soc.* **2011**, *158*, 118−121.
(37) Dorenbos, P. *J. Lumin.* **2003**, *104*, 239.
(38) Kim, J.; Kwon, A.; Park, Y.; Choi, J.; Park, H.; Kim, G. *J. Lumin.* **2007**, *583*, 122−123.
(39) Varshini, Y. P. *Physica (Amsterdam)*, **1967**, *34*, 149.
(40) Shionoya, S.; Yen, W. M. *Phosphor Handbook;* CRC Press: New York, 1998.
(41) Kim, J. S.; Park, Y. H.; Kim, S. M.; Choi, J. C.; Park, H. L. *Solid State Commun.* **2005**, *133*, 445−448.